

**Figure 7.3** | Schematic of the new terminology used in this Assessment Report (AR5) for aerosol–radiation and aerosol–cloud interactions and how they relate to the terminology used in AR4. The blue arrows depict solar radiation, the grey arrows terrestrial radiation and the brown arrow symbolizes the importance of couplings between the surface and the cloud layer for rapid adjustments. See text for further details.

warming simulation (Gregory et al., 2004; Figure 7.2), or to simulate the climate response with sea surface temperatures (SSTs) held fixed (Hansen et al., 2005). The former can be complicated by natural variability or time-varying feedbacks, while the non-zero  $\Delta T$  from land warming complicates the latter. Both methods are used in this chapter.

Figure 7.3 links the former terminology of aerosol direct, semi-direct and indirect effects with the new terminology used in this chapter and in Chapter 8. The RF from aerosol–radiation interactions (abbreviated RFari) encompasses radiative effects from anthropogenic aerosols before any adjustment takes place and corresponds to what is usually referred to as the aerosol direct effect. Rapid adjustments induced by aerosol radiative effects on the surface energy budget, the atmospheric profile and cloudiness contribute to the ERF from aerosol–radiation interactions (abbreviated ERFari). They include what has earlier been referred to as the semi-direct effect. The RF from aerosol–cloud interactions (abbreviated RFaci) refers to the instantaneous effect on cloud albedo due to changing concentrations of cloud condensation and ice nuclei, also known as the Twomey effect. All subsequent changes to the cloud lifetime and thermodynamics are rapid adjustments, which contribute to the ERF from aerosol–cloud interactions (abbreviated ERFaci). RFaci is a theoretical construct that is not easy to separate from other aerosol–cloud interactions and is therefore not quantified in this chapter.

#### 7.1.4 Chapter Roadmap

For the first time in the IPCC WGI assessment reports, clouds and aerosols are discussed together in a single chapter. Doing so allows us to assess, and place in context, recent developments in a large and growing area of climate change research. In addition to assessing cloud feedbacks and aerosol forcings, which were covered in previous assessment reports in a less unified manner, it becomes possible to assess understanding of the multiple interactions among aerosols,

clouds and precipitation and their relevance for climate and climate change. This chapter assesses the climatic roles and feedbacks of water vapour, lapse rate and clouds (Section 7.2), discusses aerosol–radiation (Section 7.3) and aerosol–cloud (Section 7.4) interactions and quantifies the resulting aerosol RF on climate (Section 7.5). It also introduces the physical basis for the precipitation responses to aerosols and climate changes (Section 7.6) noted later in the Report, and assesses geoengineering methods based on solar radiation management (Section 7.7).

## 7.2 Clouds

This section summarizes our understanding of clouds in the current climate from observations and process models; advances in the representation of cloud processes in climate models since AR4; assessment of cloud, water vapour and lapse rate feedbacks and adjustments; and the RF due to clouds induced by moisture released by two anthropogenic processes (air traffic and irrigation). Aerosol–cloud interactions are assessed in Section 7.4. The fidelity of climate model simulations of clouds in the current climate is assessed in Chapter 9.

### 7.2.1 Clouds in the Present-Day Climate System

#### 7.2.1.1 Cloud Formation, Cloud Types and Cloud Climatology

To form a cloud, air must cool or moisten until it is sufficiently supersaturated to activate some of the available condensation or freezing nuclei. Clouds may be composed of liquid water (possibly supercooled), ice or both (mixed phase). The nucleated cloud particles are initially very small, but grow by vapour deposition. Other microphysical mechanisms dependent on the cloud phase (e.g., droplet collision and coalescence for liquid clouds, riming and Wegener–Bergeron–Findeisen processes for mixed-phase clouds and crystal aggregation in ice clouds)

can produce a broader spectrum of particle sizes and types; turbulent mixing produces further variations in cloud properties on scales from kilometres to less than a centimetre (Davis et al., 1999; Bodenschatz et al., 2010). If and when some of the droplets or ice particles become large enough, these will fall out of the cloud as precipitation.

Atmospheric flows often organize convection and associated clouds into coherent systems having scales from tens to thousands of kilometres, such as cyclones or frontal systems. These represent a significant modelling and theoretical challenge, as they are usually too large to represent within the limited domains of cloud-resolving models (Section 7.2.2.1), but are also not well resolved nor parameterized by most climate models; this gap, however, is beginning to close (Section 7.2.2.2). Finally, clouds and cloud systems are organized by larger-scale circulations into different regimes such as deep convection near the equator, subtropical marine stratocumulus, or mid-latitude storm tracks guided by the tropospheric westerly jets. Figure 7.4 shows a selection of widely occurring cloud regimes schematically and as they might appear in a typical geostationary satellite image.

New satellite sensors and new analysis of previous data sets have given us a clearer picture of the Earth's clouds since AR4. A notable example

is the launch in 2006 of two coordinated, active sensors, the Cloud Profiling Radar (CPR) on the CloudSat satellite (Stephens et al., 2002) and the Cloud–Aerosol Lidar with Orthogonal Polarization (CALIOP) on board the Cloud–Aerosol Lidar and Infrared Pathfinder Satellite Observations (CALIPSO) satellite (Winker et al., 2009). These sensors have significantly improved our ability to quantify vertical profiles of cloud occurrence and water content (see Figures 7.5 and 7.6), and complement the detection capabilities of passive multispectral sensors (e.g., Stubenrauch et al., 2010; Chan and Comiso, 2011). Satellite cloud-observing capacities are reviewed by Stubenrauch et al. (2013).

Clouds cover roughly two thirds of the globe (Figure 7.5a, c), with a more precise value depending on both the optical depth threshold used to define cloud and the spatial scale of measurement (Wielicki and Parker, 1992; Stubenrauch et al., 2013). The mid-latitude oceanic storm tracks and tropical precipitation belts are particularly cloudy, while continental desert regions and the central subtropical oceans are relatively cloud-free. Clouds are composed of liquid at temperatures above 0°C, ice below about –38°C (e.g., Koop et al., 2000), and either or both phases at intermediate temperatures (Figure 7.5b). Throughout most of the troposphere, temperatures at any given altitude are usually warmer in the tropics, but clouds also extend higher there such that ice

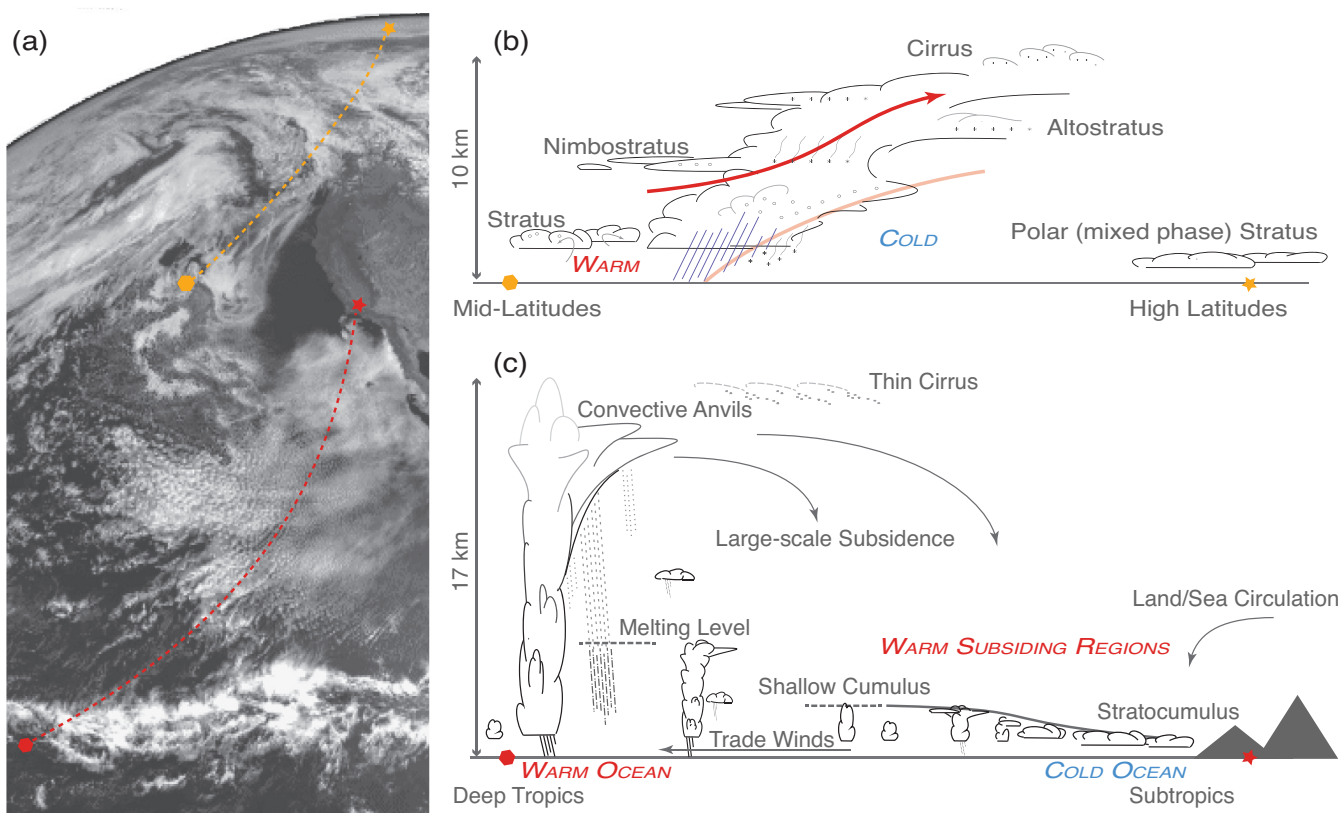


**Figure 7.4 |** Diverse cloud regimes reflect diverse meteorology. (a) A visible-wavelength geostationary satellite image shows (from top to bottom) expanses and long arcs of cloud associated with extratropical cyclones, subtropical coastal stratocumulus near Baja California breaking up into shallow cumulus clouds in the central Pacific and mesoscale convective systems outlining the Pacific Intertropical Convergence Zone (ITCZ). (b) A schematic section along the dashed line from the orange star to the orange circle in (a), through a typical warm front of an extratropical cyclone. It shows (from right to left) multiple layers of upper-tropospheric ice (cirrus) and mid-tropospheric water (altostratus) cloud in the upper-tropospheric outflow from the frontal zone, an extensive region of nimbostratus associated with frontal uplift and turbulence-driven boundary layer cloud in the warm sector. (c) A schematic section along the dashed line from the red star to the red circle in (a), along the low-level trade wind flow from a subtropical west coast of a continent to the ITCZ. It shows (from right to left) typical low-latitude cloud mixtures, shallow stratocumulus trapped under a strong subsidence inversion above the cool waters of the oceanic upwelling zone near the coast and shallow cumulus over warmer waters further offshore transitioning to precipitating cumulonimbus cloud systems with extensive cirrus anvils associated with rising air motions in the ITCZ.

cloud amounts are no less than those at high latitudes. At any given time, most clouds are not precipitating (Figure 7.5d).

In this chapter cloud above the 440 hPa pressure level is considered 'high', that below the 680 hPa level 'low', and that in-between is considered 'mid-level'. Most high cloud (mainly cirrus and deep cumulus outflows) occurs near the equator and over tropical continents, but can also be seen in the mid-latitude storm track regions and over mid-latitude continents in summer (Figure 7.6a, e); it is produced by the storms generating most of the global rainfall in regions where tropospheric air motion is upward, such that dynamical, rainfall and high-cloud fields closely resemble one another (Figure 7.6d, h). Mid-level cloud (Figure 7.6b, f), comprising a variety of types, is prominent in the storm tracks and some occurs in the Intertropical Convergence Zone (ITCZ). Low cloud (Figure 7.6c, g), including shallow cumulus and stratiform cloud, occurs over essentially all oceans but is most prevalent over cooler subtropical oceans and in polar regions. It is less common over land, except at night and in winter.

Overlap between cloud layers has long been an issue both for satellite (or ground-based) detection and for calculating cloud radiative effects. Active sensors show more clearly that low clouds are prevalent in nearly all types of convective systems, and are often underestimated by models (Chepfer et al., 2008; Naud et al., 2010; Haynes et al., 2011). Cloud layers at different levels overlap less often than typically assumed in General Circulation Models (GCMs), especially

over high-latitude continents and subtropical oceans (Naud et al., 2008; Mace et al., 2009), and the common assumption that the radiative effects of precipitating ice can be neglected is not necessarily warranted (Waliser et al., 2011). New observations have led to revised treatments of overlap in some models, which significantly affects cloud radiative effects (Pincus et al., 2006; Shonk et al., 2012). Active sensors have also been useful in detecting low-lying Arctic clouds over sea ice (Kay et al., 2008), improving our ability to test climate model simulations of the interaction between sea ice loss and cloud cover (Kay et al., 2011).

### 7.2.1.2 Effects of Clouds on the Earth's Radiation Budget

The effect of clouds on the Earth's present-day top of the atmosphere (TOA) radiation budget, or cloud radiative effect (CRE), can be inferred from satellite data by comparing upwelling radiation in cloudy and non-cloudy conditions (Ramanathan et al., 1989). By enhancing the planetary albedo, cloudy conditions exert a global and annual shortwave cloud radiative effect (SWCRE) of approximately  $-50 \text{ W m}^{-2}$  and, by contributing to the greenhouse effect, exert a mean longwave effect (LWCRE) of approximately  $+30 \text{ W m}^{-2}$ , with a range of 10% or less between published satellite estimates (Loeb et al., 2009). Some of the apparent LWCRE comes from the enhanced water vapour coinciding with the natural cloud fluctuations used to measure the effect, so the true cloud LWCRE is about 10% smaller (Sohn et al., 2010). The net global mean CRE of approximately  $-20 \text{ W m}^{-2}$  implies a net cooling

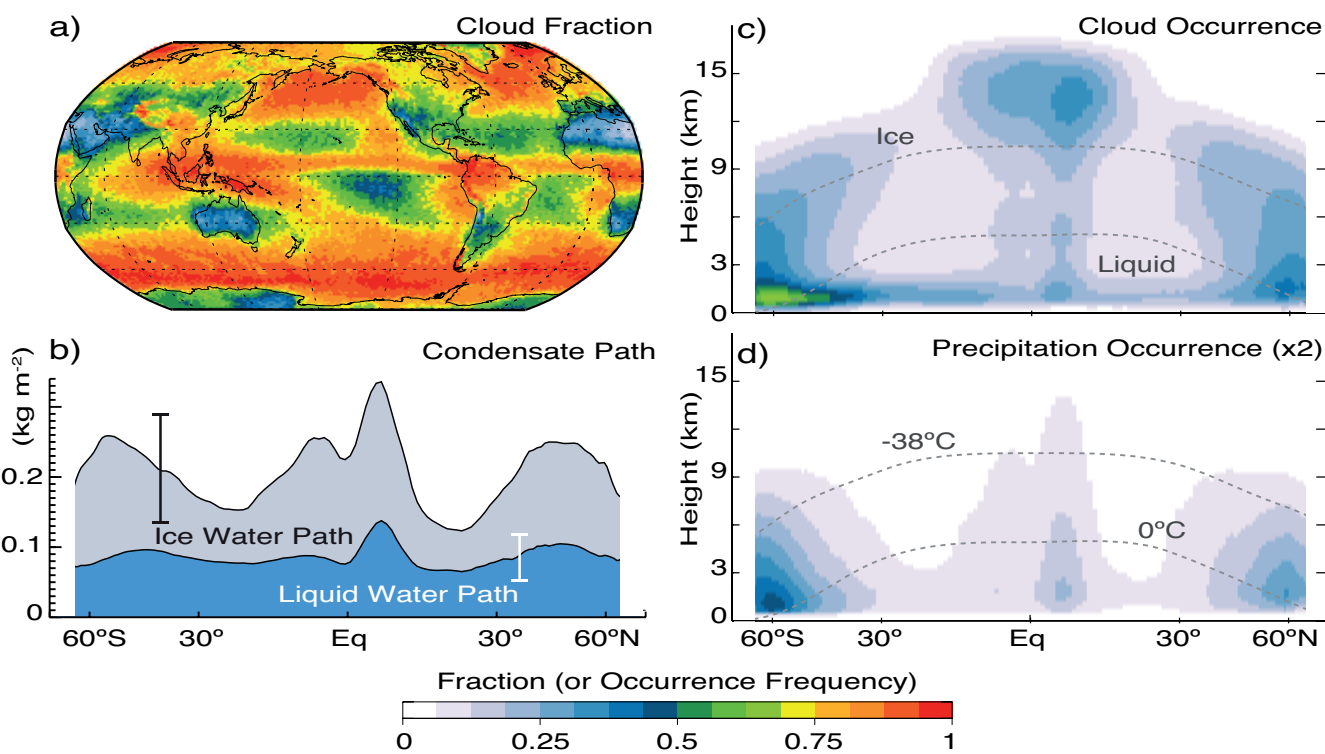


**Figure 7.5 |** (a) Annual mean cloud fractional occurrence (CloudSat/CALIPSO 2B-GEOPROF-LIDAR data set for 2006–2011; Mace et al., 2009). (b) Annual zonal mean liquid water path (blue shading, microwave radiometer data set for 1988–2005 from O'Dell et al. (2008)) and total water path (ice path shown with grey shading, from CloudSat 2C-ICE data set for 2006–2011 from Deng et al. (2010)) over oceans. The 90% uncertainty ranges, assessed to be approximately 60 to 140% of the mean for the liquid and total water paths, are schematically indicated by the error bars. (c–d) latitude-height sections of annual zonal mean cloud (including precipitation falling from cloud) occurrence and precipitation (attenuation-corrected radar reflectivity  $>0 \text{ dBZ}$ ) occurrence; the latter has been doubled to make use of a common colour scale (2B-GEOPROF-LIDAR data set). The dashed curves show the annual mean  $0^\circ\text{C}$  and  $-38^\circ\text{C}$  isotherms.

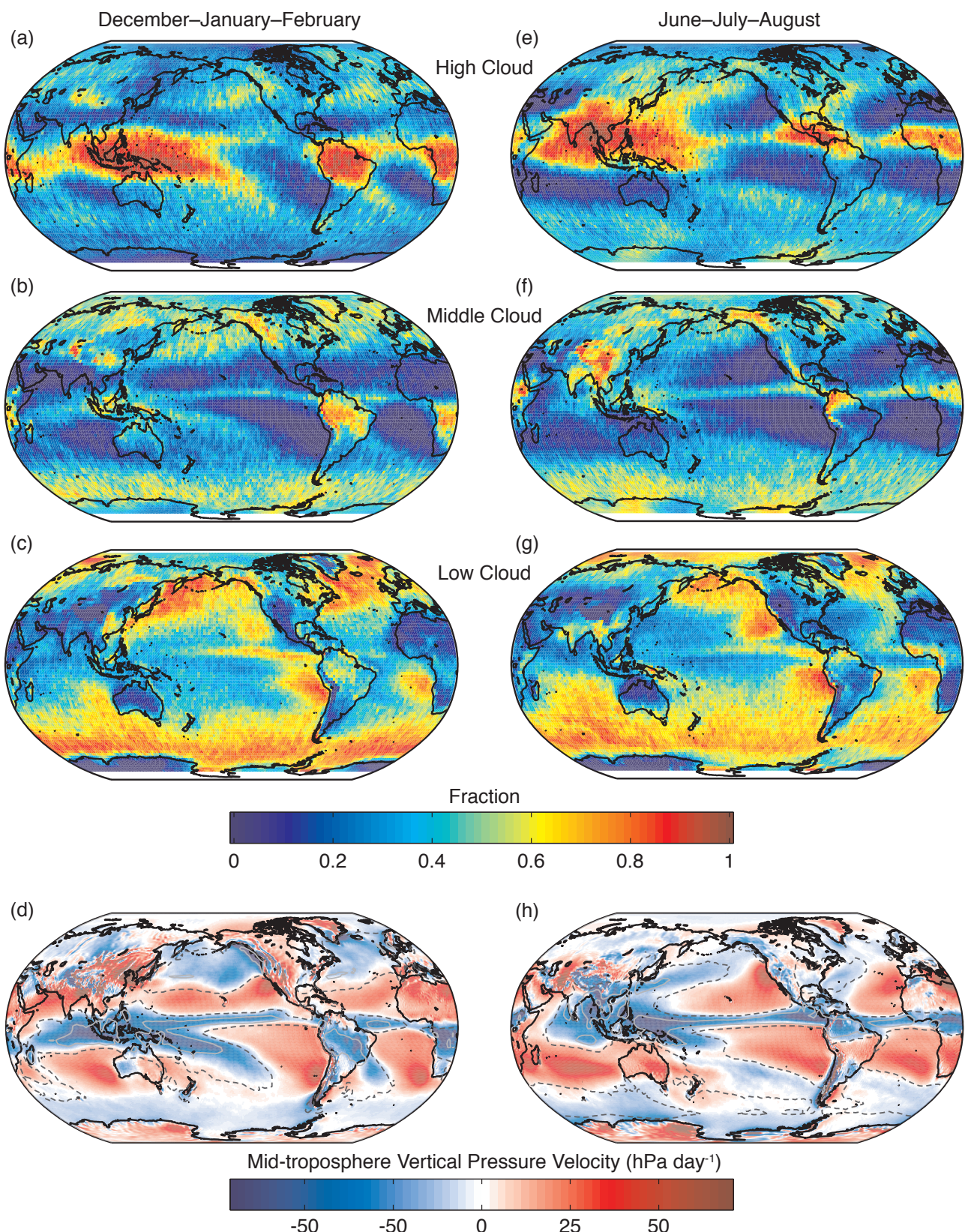


**Figure 7.6 |** (a–d) December–January–February mean high, middle and low cloud cover from CloudSat/CALIPSO 2B-GEOPROF R04 and 2B-GEOPROF-LIDAR P1.R04 data sets for 2006–2011 (Mace et al., 2009), 500 hPa vertical pressure velocity (colours, from ERA-Interim for 1979–2010; Dee et al., 2011), and Global Precipitation Climatology Project (GPCP) version 2.2 precipitation rate (1981–2010, grey contours at 3  $\text{mm day}^{-1}$  in dash and 7  $\text{mm day}^{-1}$  in solid); (e–h) same as (a–d), except for June–July–August. For low clouds, the GCM-Oriented CALIPSO Cloud Product (GOCCP) data set for 2007–2010 (Chepfer et al., 2010) is used at locations where it indicates a larger fractional cloud cover, because the GEOPROF data set removes some clouds with tops at altitudes below 750 m. Low cloud amounts are probably underrepresented in regions of high cloud (Chepfer et al., 2008), although not as severely as with earlier satellite instruments.

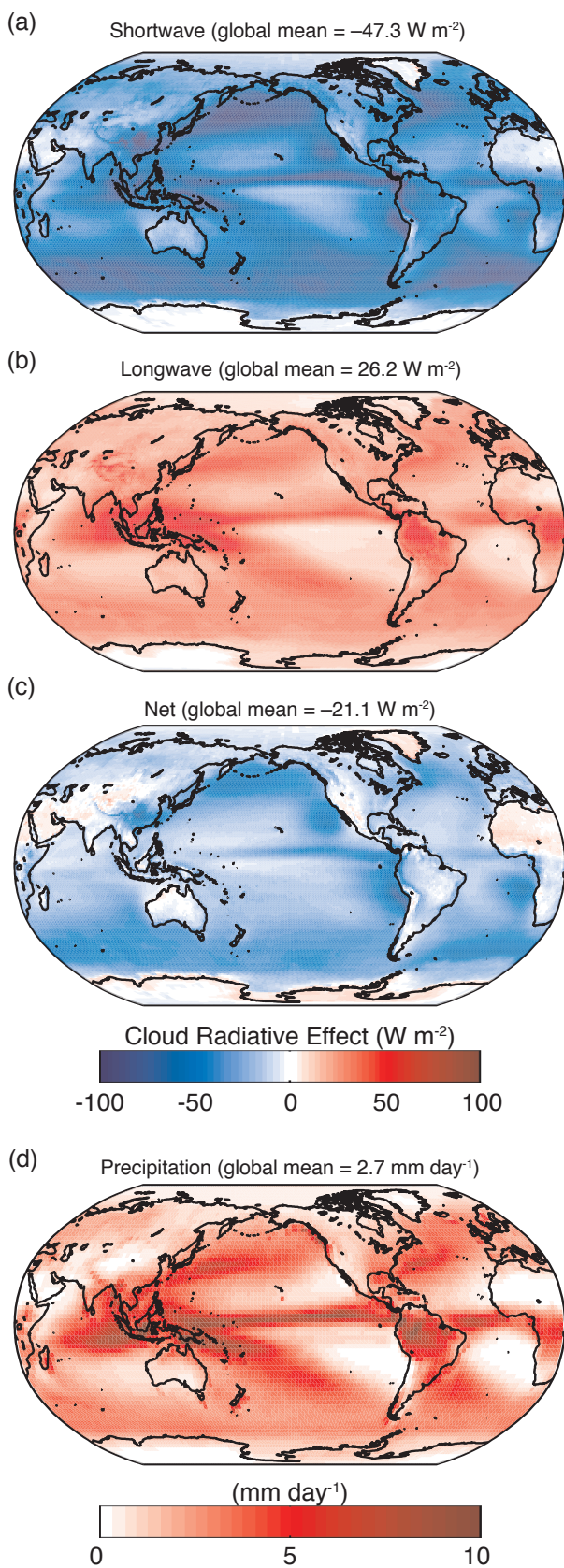


**Figure 7.7 |** Distribution of annual-mean top of the atmosphere (a) shortwave, (b) longwave, (c) net cloud radiative effects averaged over the period 2001–2011 from the Clouds and the Earth's Radiant Energy System (CERES) Energy Balanced and Filled (EBAF) Ed2.6r data set (Loeb et al., 2009) and (d) precipitation rate (1981–2000 average from the GPCP version 2.2 data set; Adler et al., 2003).

effect of clouds on the current climate. Owing to the large magnitudes of the SWCRE and LWCRE, clouds have the potential to cause significant climate feedback (Section 7.2.5). The sign of this feedback on climate change cannot be determined from the sign of CRE in the current climate, but depends instead on how climate-sensitive the properties are that govern the LWCRE and SWCRE.

The regional patterns of annual-mean TOA CRE (Figure 7.7a, b) reflect those of the altitude-dependent cloud distributions. High clouds, which are cold compared to the clear-sky radiating temperature, dominate patterns of LWCRE, while the SWCRE is sensitive to optically thick clouds at all altitudes. SWCRE also depends on the available sunlight, so for example is sensitive to the diurnal and seasonal cycles of cloudiness. Regions of deep, thick cloud with large positive LWCRE and large negative SWCRE tend to accompany precipitation (Figure 7.7d), showing their intimate connection with the hydrological cycle. The net CRE is negative over most of the globe and most negative in regions of very extensive low-lying reflective stratus and stratocumulus cloud such as the mid-latitude and eastern subtropical oceans, where SWCRE is strong but LWCRE is weak (Figure 7.7c). In these regions, the spatial distribution of net CRE on seasonal time scales correlates strongly with measures of low-level stability or inversion strength (Klein and Hartmann, 1993; Williams et al., 2006; Wood and Bretherton, 2006; Zhang et al., 2010).

Clouds also exert a CRE at the surface and within the troposphere, thus affecting the hydrological cycle and circulation (Section 7.6), though this aspect of CRE has received less attention. The net downward flux of radiation at the surface is sensitive to the vertical and horizontal distribution of clouds. It has been estimated more accurately through radiation budget measurements and cloud profiling (Kato et al., 2011). Based on these observations, the global mean surface downward long-wave flux is about  $10 \text{ W m}^{-2}$  larger than the average in climate models, probably due to insufficient model-simulated cloud cover or lower tropospheric moisture (Stephens et al., 2012). This is consistent with a global mean precipitation rate in the real world somewhat larger than current observational estimates.

## 7.2.2 Cloud Process Modelling

Cloud formation processes span scales from the sub-micrometre scale of CCN, to cloud-system scales of up to thousands of kilometres. This range of scales is impossible to resolve with numerical simulations on computers, and this is not expected to change in the foreseeable future. Nonetheless progress has been made through a variety of modelling strategies, which are outlined briefly in this section, followed by a discussion in Section 7.2.3 of developments in representing clouds in global models. The implications of these discussions are synthesized in Section 7.2.3.5.

### 7.2.2.1 Explicit Simulations in Small Domains

High-resolution models in small domains have been widely used to simulate interactions of turbulence with various types of clouds. The grid spacing is chosen to be small enough to resolve explicitly the dominant turbulent eddies that drive cloud heterogeneity, with the effects of smaller-scale phenomena parameterized. Such models can be run in